This article was published in

A. Säynätjoki, M. Mulot, K. Vynck, D. Cassagne, J. Ahopelto, and H. Lipsanen. 2008. Properties, applications and fabrication of photonic crystals with ring-shaped holes in silicon-on-insulator. Photonics and Nanostructures – Fundamentals and Applications, volume 6, pages 42-46.

Available online at www.sciencedirect.com
ScienceDirect
Photonics and Nanostructures – Fundamentals and Applications 6 (2008) 42–46
PHOTONICS AND NANOSTRUCTURES Fundamentals and Applications
www.elsevier.com/locate/photonics

Properties, applications and fabrication of photonic crystals with ring-shaped holes in silicon-on-insulator

A. Säynätjoki [a,*], M. Mulot [a,b], K. Vynck [c], D. Cassagne [c], J. Ahopelto [b], H. Lipsanen [a]

[a] *Helsinki University of Technology (TKK), Micro and Nanosciences Laboratory, Micronova, Tietotie 3, FIN-02015 Espoo, Finland*
[b] *VTT Information Technology, Micronova, P.O. Box 1208, FIN-02044 VTT, Finland*
[c] *Groupe d'Etude des Semiconducteurs, UMR 5650 CNRS, Université Montpellier II, CC074 Place Eugéne Bataillon, 34095 Montpellier Cedex 05, France*

Received 17 June 2007; received in revised form 21 August 2007; accepted 4 September 2007
Available online 8 September 2007

Abstract

We show that photonic crystals with ring-shaped holes (RPhCs) exhibit superior properties compared to conventional photonic crystals (PhCs). At low air-fill factors RPhCs can have a larger bandgap than conventional PhCs. Moreover, RPhC waveguides with both high group index and small group velocity dispersion can be designed. RPhC waveguides are also more sensitive to external refractive index changes, which is attractive for sensor applications. Finally we set up a procedure to pattern RPhCs in silicon-on-insulator.

PACS : 42.15.Eq; 42.70.Qs; 42.82.−m; 42.82.Cr; 42.82.Et; 42.82.Gw

Keywords: Guided waves; Integrated optics materials; Optical systems design; Waveguides; Photonic integrated circuits; Dispersion; Photonic crystals

1. Introduction

Planar photonic crystals (PhCs) are structures with a periodic variation of the dielectric constant in two dimensions [1]. From the periodicity, a forbidden wavelength range for photons can arise (i.e., photonic bandgap). PhCs are used to realize various building blocks (e.g. waveguides, cavities or mirrors) that can be functionalized or combined to realize high-performance devices for integrated optics: filters, lasers, splitters or sensors to cite only a few.

Lattices of circular holes are the dominating PhC geometries. We choose to study photonic crystals based on ring-shaped holes (RPhCs). It has been demonstrated earlier that RPhCs possess polarization-independent photonic bandgap [2]. We also have shown that some RPhC waveguides (RPhCWs) exhibit low group velocity dispersion [3,4].

Fig. 1 shows a schematic of an RPhC. The ring is defined by its inner and outer radii R_{in} and R_{out}. Hence two parameters are available for tailoring of the photonic band structure. A circular hole corresponds in fact to the limit case $R_{in} = 0$.

In this paper, we investigate different properties of RPhCs, refine our results on slow light RPhCWs and show that RPhCWs can be used as efficient biosensors. We also demonstrate fabrication of such structures. We

* Corresponding author.
E-mail address: antti.saynatjoki@tkk.fi (A. Säynätjoki).

1569-4410/$ – see front matter © 2007 Elsevier B.V. All rights reserved.
doi:10.1016/j.photonics.2007.09.001

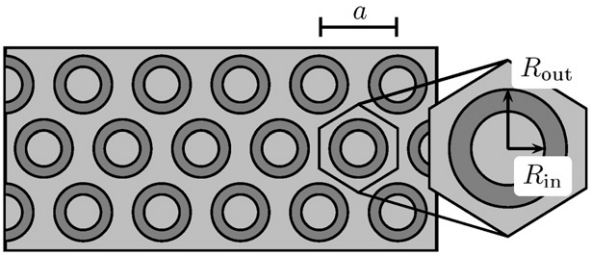

Fig. 1. Sketch of an RPhC.

consider a thin silicon slab (<500 nm) on silica as material platform. It is commercially available as silicon-on-insulator (SOI) wafers. From the fabrication point of view, thin slabs require only shallow etching, which is convenient in the case of high aspect ratio structures such as RPhCs.

2. Properties and applications

2.1. Bandgap width and frequency

In order to study the bandgap of the RPhCs, their band structures were calculated with the MIT Photonic Bands software, which uses the plane wave expansion (PWE) method [5]. In the 2D simulations of Figs. 2 and 3, we take $n_{eff} = 2.835$ as the background refractive index. This corresponds to the effective index of the fundamental guided TE mode in a 220 nm thick silicon slab on silicon dioxide at a wavelength of 1550 nm. All the simulations were carried out for the TE polarization.

Figs. 2 and 3 show the bandgap edge frequencies and the gap to mid-gap ratio, respectively, as a function of R_{out}. The graphs are plotted for different values of the air-fill factor f_{air}, which is defined as the area of the air hole divided by the area of a primitive cell of the RPhC lattice:

$$f_{air} = \frac{2\pi}{\sqrt{3}a^2}(R_{out}^2 - R_{in}^2), \quad (1)$$

where a is the lattice constant. The dots in Figs. 2 and 3 correspond to the case where $R_{in} = 0$, i.e., where the hole is circular.

When $R_{out} < 0.38a$, the top and bottom edges of the bandgap are at higher frequencies in the RPhC than in the conventional PhC with the same f_{air} (Fig. 2). This means that the eigenmodes above and below the bandgap in the RPhC concentrate more of their energy in the air region, compared to the conventional PhC.

For $f_{air} < 30\%$, it is possible to find values of R_{out} for which the gap width in the RPhC is larger than in the conventional PhC (Fig. 3). The larger bandgap is an advantage in mirrors and cavities, where modes deep inside the bandgap experience higher reflectivity.

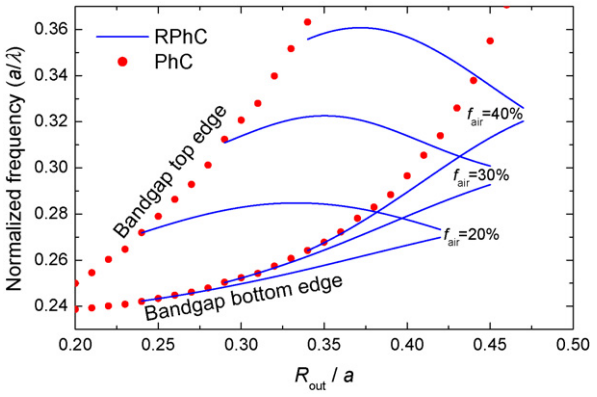

Fig. 2. Bandgap top and bottom edge frequencies for the TE polarization in an RPhC as a function of ring outer radius R_{out} at different air-fill factors. The dots correspond to a conventional PhC with radius R_{out} ($R_{in} = 0$).

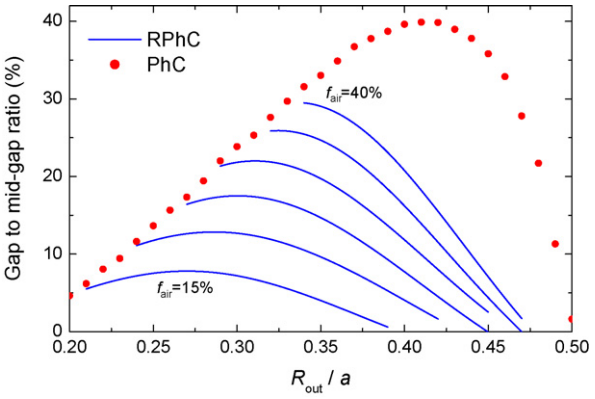

Fig. 3. Gap to mid-gap ratio for the TE polarization in an RPhC as a function of ring outer radius R_{out}. The solid lines correspond to air-fill factors from 15% to 40% with a step of 5% units. The dots correspond to a conventional PhC.

2.2. Slow light in RPhC waveguides

Guided modes in PhC waveguides (PhCWs) exhibit decreased group velocity near the Brillouin zone edge (i.e., when the propagation constant β of the guided mode is close to π/a) [6–10]. This enhances light–matter interaction and nonlinearities, which may be utilized to realize more compact integrated optics devices. However, slow modes usually have a very high group velocity dispersion, which leads to optical signal degradation in telecommunication systems. Therefore, it is necessary to tailor the dispersion properties of the slow mode [11–13].

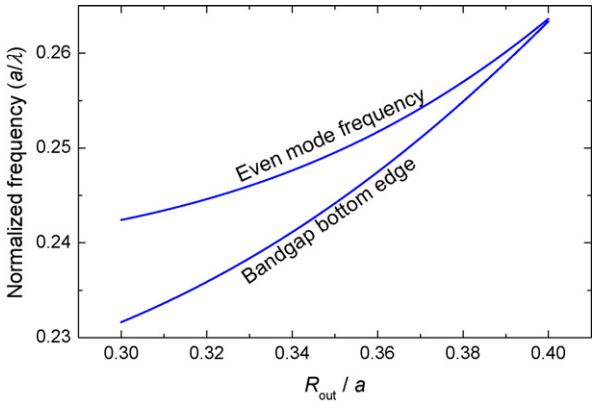

Fig. 4. Frequencies of the bandgap bottom edge and the even guided mode at $\beta = 0.35(2\pi/a)$ as a function of ring outer radius R_{out} in a W1 RPhCW with a ring width $R_{out} - R_{in} = 0.15a$, in a silicon slab with a thickness $h = 1.02a$.

As shown in Fig. 2, the bandgap bottom edge frequency of the RPhC is increased with increasing R_{out}. The frequency of the guided mode in the W1 RPhCW increases at a lesser rate than the bandgap edge frequency (Fig. 4). Therefore, with $R_{out} > 0.37a$, the bandgap bottom edge gets close to the guided mode in the dispersion diagram when $0.35(2\pi/a) < \beta < 0.4(2\pi/a)$ (see the left graph of Fig. 5).

Close to the bandgap edge the modefield becomes wider, which enhances the effect of the periodic RPhC lattice and extends the low group velocity region further away from the Brillouin zone edge [4]. This is illustrated in the right graph of Fig. 5, which shows the wavelength dependence of the group index $n_g = (c/v_g)$ in a W1 RPhC waveguide. The group index is nearly constant around a value of 55 over a wavelength range of 5 nm. The group index in a conventional PhCW with the same f_{air}, which is plotted for comparison, increases exponentially in the vicinity of the cut-off wavelength of the slow mode.

The graphs in Figs. 4 and 5 were simulated in 3D with the PWE method [5]. The silicon slab thickness h used in the calculations is $1.02a$, corresponding to about 400 nm. The relatively thick slab thickness is chosen in order to increase the effective refractive index of the guided mode. With higher n_{eff}, a larger part of the dispersion curve of the mode is below the light line, in which case the mode is intrinsically lossless.

The group index values reported here are higher than in [4] for the same waveguide. Contrarily to the effective index approximation used in [4], the 3D method used here takes into account the dispersion of the silicon slab, which results in larger n_g values.

2.3. Sensor applications

The cut-off frequency of the even guided mode in PhCWs is very sensitive to refractive index variation in the ambient medium. This property can be used for biochemical sensing [14]. In the following we make a comparison between sensitivity of the cut-off frequency in an RPhCW and a PhCW, both fabricated into the SOI substrate with $f_{air} \approx 34\%$ and $\lambda_{co} \approx 1570$ nm. The comparison is carried out using 3D simulations with the MIT photonic bands package [5]. We consider that the volume above the waveguide and inside the holes is filled with a gas or a liquid with refractive index n_a.

Fig. 6 shows the cut-off wavelength λ_{co} in two waveguides as a function of n_a. The change in the cut-off wavelength as a function of n_a is nearly linear between $n_a = 1.00$ and $n_a = 1.10$. If we define the sensitivity as the relative cut-off shift $\Delta\lambda_{co}/\lambda_{co}$ in %

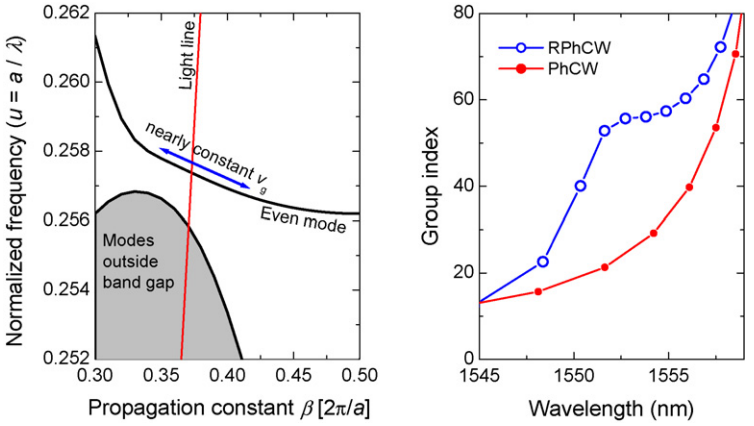

Fig. 5. Dispersion relation and group index in a W1 RPhCW with $a = 400$ nm, $R_{out} = 0.385a$ and $R_{in} = 0.235a$. Group index in a W1 PhCW with $a = 375$ nm and $R = 0.305a$ is plotted for reference. For both waveguides, $f_{air} \approx 34\%$ and the silicon slab thickness $h = 1.02a$.

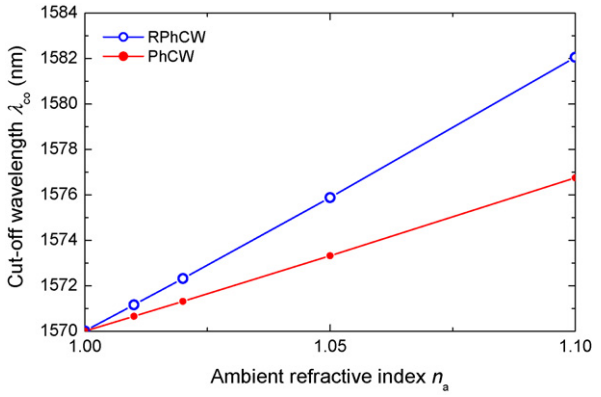

Fig. 6. Calculated cut-off wavelength as a function of the ambient refractive index n_a for a W1 PhCW and a W1 RPhCW etched in SOI. For the RPhCW: $a = 405$ nm, $R_{out} = 0.385a$ and $R_{in} = 0.235a$. For the PhCW: $a = 380$ nm and $R = 0.305a$. For both waveguides $f_{air} \approx 34\%$ and $h = a$.

induced by an ambient refractive index change $\Delta n_a = 0.01$, the sensitivity is 0.073% for the RPhCW and 0.042% for the PhCW. Thus, the RPhCW is nearly twice as sensitive as the conventional PhCW with the same f_{air}.

Fig. 7 shows the sensitivity of an RPhCW as a function of R_{out} for different air-fill factors. The sensitivity of a conventional PhCW as a function of the hole radius is plotted in comparison. The 2D PWE simulations were carried out with an effective refractive index $n_{eff} = 3.178$, equivalent to a 400 nm thick silicon layer on SiO_2 at $\lambda = 1550$ nm.

The sensitivity of the conventional PhCW is nearly constant for a hole radius smaller than $0.4a$. For a hole radius larger than $0.4a$, the sensitivity eventually increases. However, PhCs with such large circular holes are difficult to manufacture due to the very thin walls between neighboring holes. In the case of RPhCWs, sensitivity increases with decreasing f_{air} and with increasing R_{out}. In other words the rings should be as narrow as possible for optimal sensitivity. The example of Fig. 6 has a ring width $R_{out} - R_{in}$ of 60 nm. We show next that such narrow rings can be manufactured by electron beam lithography.

3. Fabrication

Insets in Fig. 8 show scanning electron micrographs of RPhCs manufactured on commercial SOI wafers. After thermal oxidation of a 30 nm thick SiO_2 layer for the hard mask, the top silicon layer thickness is 240 nm. A 320 nm thick layer of PMMA is spun onto the SOI wafer and the RPhCs are patterned into the PMMA with a LEO 1560 scanning electron microscope converted into an electron beam lithography system. After developing of the resist, the RPhC pattern is transferred into the SiO_2 mask. Finally, the pattern is etched into the silicon layer by reactive ion etching (RIE). The etching proceeds through the top silicon layer and stops at the bottom silica [3].

The rings are written as circular lines with the radius $(R_{out} + R_{in})/2$. The final R_{out} and R_{in} are determined by the width of the line, which depends on the beam current and the scanning speed of the beam (Fig. 8). This method intrinsically minimizes the exposure time. Hence, writing of a field of ring holes takes up to four times less time than writing of a field of circular holes with similar air-fill factor.

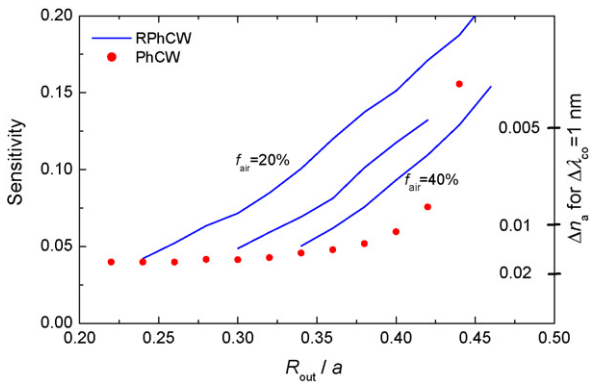

Fig. 7. Calculated sensitivity in RPhCW with $f_{air} = 20\%$, 30% and 40%. The dots correspond to a conventional PhCW with hole radius R_{out}. The sensitivity is defined as the relative cut-off shift $\Delta\lambda_{co}/\lambda_{co}$ in % induced by an ambient refractive index change Δn_a equal to 0.01. The ticks on the y axis on the right show Δn_a that induces $\Delta\lambda_{co} = 1$ nm when $\lambda_{co} = 1570$ nm.

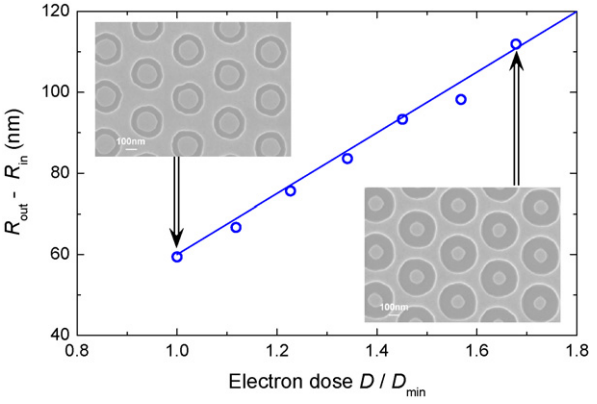

Fig. 8. Measured ring width $R_{out} - R_{in}$ after etching of the RPhC as a function of the electron dose D applied during electron beam lithography. D is expressed in Coulombs per unit length in the line exposure mode. D_{min} is the smallest dose that yields well-defined rings. The insets are scanning electron micrographs of RPhC patterned with different doses. The period of the RPhC is 440 nm.

4. Conclusion

We showed that for small air-fill factors ($f_{\text{air}} < 30\%$) it is possible to achieve a larger bandgap for RPhCs than for conventional PhCs. This can be useful to improve the performance of the PhC mirrors and cavities in the SOI material platform. We also showed that in RPhCs with $R_{\text{out}} < 0.38a$ the eigenmodes at the edges of the photonic bandgap are shifted to higher frequencies compared to the conventional PhC with the same f_{air}. We designed a W1 waveguide based on ring-shaped holes with a constant n_{g} of about 55 over a wavelength range of 5 nm. This is of high interest in optical telecommunications, where active and nonlinear integrated optics devices with a sufficient bandwidth and small dispersion are needed. Moreover, we demonstrated that the sensitivity of the cut-off wavelength to external refractive index variation is nearly double in an RPhCW compared to a conventional PhCW with the same f_{air}. This improvement is directly relevant for biosensing applications where, for example, biochemical reactions are monitored by measuring small refractive index change in the reaction medium. Finally, using an electron beam writer in line exposure mode and RIE etching, we successfully patterned RPhCs with a linewidth as narrow as 60 nm into a 240 nm thick silicon slab.

Acknowledgements

This work was financed by the European Union under project PHAT, by the Academy of Finland under the PHC-OPTICS project and graduate school GETA.

References

[1] J.D. Joannopoulos, R.D. Meade, J.N. Winn, Photonic Crystals: Molding the Flow of Light, Princeton University Press, Princeton, NJ, USA, 1995.

[2] H. Kurt, D.S. Citrin, Annular photonic crystals, Opt. Express 13 (2005) 10316–10326.

[3] M. Mulot, A. Säynätjoki, S. Arpiainen, H. Lipsanen, J. Ahopelto, Slow light propagation in photonic crystal waveguides with ring-shaped holes, J. Opt. A: Pure Appl. Opt. 9 (2007) S415–S418.

[4] A. Säynätjoki, M. Mulot, J. Ahopelto, H. Lipsanen, Dispersion engineering of photonic crystal waveguides with ring-shaped holes, Opt. Express 15 (2007) 8323–8328.

[5] S. Johnson, J.D. Joannopoulos, Block-iterative frequency-domain methods for Maxwell's equations in a planewave basis, Opt. Express 8 (2001) 173–190.

[6] M. Notomi, K. Yamada, A. Shinya, J. Takahashi, C. Takahashi, I. Yokohama, Extremely large group-velocity dispersion of line-defect waveguides in photonic crystal slabs, Phys. Rev. Lett. 87 (2001) 253902–253911.

[7] X. Letartre, C. Seassal, C. Grillet, P. Rojo-Romeo, P. Viktorovitch, M. Le Vassor d'Yerville, D. Cassagne, C. Jouanin, Group velocity and propagation losses measurement in a single-line photonic-crystal waveguide on InP membranes, Appl. Phys. Lett. 79 (2001) 2312–2314.

[8] M. Notomi, A. Shinya, S. Mitsugi, E. Kuramochi, H-Y. Ryu, Waveguides, resonators and their coupled elements in photonic crystal slabs, Opt. Express 12 (2004) 1551–1561.

[9] H. Gersen, T.J. Karle, R.J.P. Engelen, W. Bogaerts, J.P. Korterik, N.F. van Hulst, T.F. Krauss, L. Kuipers, Real-space observation of ultraslow light in photonic crystal waveguides, Phys. Rev. Lett. 94 (2005) 073903.

[10] Y.A. Vlasov, M. O'Boyle, H.F. Hamann, S.J. McNab, Active control of slow light on a chip with photonic crystal waveguides, Nature 438 (2005) 65–69.

[11] M.D. Settle, R.J.P. Engelen, M. Salib, A. Michaeli, L. Kuipers, T.F. Krauss, Flatband slow light in photonic crystals featuring spatial pulse compression and terahertz bandwidth, Opt. Express 15 (2007) 219–226.

[12] L.H. Frandsen, A.V. Lavrinenko, J. Fage-Pedersen, P.I. Borel, Photonic crystal waveguides with semi-slow light and tailored dispersion properties, Opt. Express 14 (2006) 9444–9450.

[13] A. Jafarpour, A. Adibi, Y. Xu, R.K. Lee, Mode dispersion in biperiodic photonic crystal waveguides, Phys. Rev. B 68 (2003) 233102.

[14] N. Skivesen, A. Tétu, M. Kristensen, J. Kjems, L.H. Frandsen, P.I. Borel, Photonic-crystal waveguide biosensor, Opt. Express 15 (2007) 3169–3176.